Published in Journal of Applied Physics 113, issue 6, 064501/1-8, 2013
which should be used for any reference to this work

Low-temperature indium-bonded alkali vapor cell for chip-scale atomic clocks

R. Straessle,[1,a)] M. Pellaton,[2] C. Affolderbach,[2] Y. Pétremand,[1,b)] D. Briand,[1] G. Mileti,[2] and N. F. de Rooij[1]
[1]*Sensors, Actuators and Microsystems Laboratory (SAMLAB), Institute of Microengineering (IMT), Ecole Polytechnique Fédérale de Lausanne (EPFL), 2000 Neuchâtel, Switzerland*
[2]*Laboratoire Temps-Fréquence (LTF), Institut de Physique, Université de Neuchâtel, 2000 Neuchâtel Switzerland*

A low-temperature sealing technique for micro-fabricated alkali vapor cells for chip-scale atomic clock applications is developed and evaluated. A thin-film indium bonding technique was used for sealing the cells at temperatures of $\leq 140\,^{\circ}\mathrm{C}$. These sealing temperatures are much lower than those reported for other approaches, and make the technique highly interesting for future micro-fabricated cells, using anti-relaxation wall coatings. Optical and microwave spectroscopy performed on first indium-bonded cells without wall coatings are used to evaluate the cleanliness of the process as well as a potential leak rate of the cells. Both measurements confirm a stable pressure inside the cell and therefore an excellent hermeticity of the indium bonding. The double-resonance measurements performed over several months show an upper limit for the leak rate of 1.5×10^{-13} mbar·l/s. This is in agreement with additional leak-rate measurements using a membrane deflection method on indium-bonded test structures.

I. INTRODUCTION

Micro-fabricated alkali vapor cells can be considered as the heart of current chip-scale atomic clock (CSAC).[1] They contain the alkali atoms of which the hyperfine splitting of the valence electron's $^2S_{1/2}$ ground state is used as reference for stabilizing the frequency of a quartz oscillator.[2] Alkali vapor cells for CSACs aim to achieve small cell sizes down to 1 mm or less, while meeting the requirements for atomic clock operation: the atmosphere inside such cells surrounding the atoms must be chemically inert with respect to the alkali atoms, well-controlled, and stable over time to ensure a minimal frequency drift of the resonance signal. Hence, the sealing of the cell has to be hermetic, and the material used should not be susceptible to outgassing during bonding nor during duty in order to maintain a clean inner atmosphere. The materials used for the cell must not interact chemically with the alkali metals; neither should they be magnetic to not distort the optical and electromagnetic measurements. Optical access from and to the atoms is required, and the cell and its packaging structure have to withstand temperatures in the 70 °C–100 °C range for mm-scale cells.

Reliable sealing of micro-fabricated alkali vapor cell with buffer gas (BG) has been demonstrated by anodic bonding[3] or glass-frit bonding,[4] at temperatures of 300 °C and >460 °C, respectively. In most atomic sensors, BG technology is used to significantly reduce spin relaxation via a decreased collision rate of the alkali atoms with the cell walls. However, in mm-scale cells where elevated BG pressures are required for obtaining a narrow linewidth of the reference transition, this technology also has its drawbacks such as reduction of the signal's amplitude (e.g., due to broadening of the optical atomic pump transitions) or reduced efficiency in the creation of atomic alignment.[5] As an alternative method to enhance the quality factor of the clock signal—and thus the short-term stability of the clock—anti-relaxation coatings have the potential to reduce the spin relaxation in the alkali cells even at very small scale.[6–8] The implementation of macroscopic alkali vapor cells equipped with anti-relaxation wall-coatings has been shown to be effective for the realization of novel atomic clocks with high frequency stability.[6,9] While not yet studied extensively, the use of such coatings is also of high interest in micro-fabricated alkali cells for miniature atomic clocks.[5,10,11]

There are two main groups of established wall-coatings: paraffins and organosilanes. Paraffins are very efficient anti-relaxation coatings but suffer from relatively low melting temperatures in the range of 70 °C to 90 °C with decreased performance above the melting temperature.[12] Organosilanes, e.g., octadecyltrichlorosilane (OTS) applied as self-assembled monolayers (SAM)[5] or multilayers,[13] are thermally stable up to 230 °C in air and can be heated up to 170 °C in the presence of Rb vapor. Above this temperature, irreversible degradation is observed.[5,13] Organosilanes' anti-relaxation properties are reported to be highly variable between different realizations as the coverage is not easy to control. Furthermore, those coatings are typically less efficient compared to paraffin, in particular in Rb cells.[5]

None of these known anti-relaxation coatings withstands the high temperatures of $\geq 300\,^{\circ}\mathrm{C}$ required for sealing of micro-fabricated alkali vapor cells that are required for the established methods of anodic or glass-frit bonding. Facing this challenge, the two solutions envisaged are either a newly engineered coating, which would withstand the high bonding

a)Electronic address: rahel.straessle@epfl.ch.
b)Present address: CSEM, Microsystems Technology Division, 2000 Neuchâtel, Switzerland.

temperature and also the high electric field of anodic bonding, or a new cell fabrication technique with reduced sealing temperature. In view of reducing the process temperatures for micro-fabricated cells, we previously reported a sealing technique based on thick indium rings.[14]

Here we report on the realization of micro-fabricated Rb vapor cells using a refined low-temperature sealing method based on thin-film indium thermo-compression bonding[15,16] that allows for improved indium purity, better control of geometry, and which requires temperatures below 140 °C only. The cell fabrication and sealing process, as well as mechanical validation results of the indium bond, are described. Laser and optical-microwave double-resonance spectroscopy are used to demonstrate the suitability of the realized cells for atomic clock applications. As any gas present in the alkali cell will broaden the observed lines both in optical absorption as well as the double-resonance spectra, the recorded spectra are used to validate the indium bonding technique in terms of hermeticity. By recording the center frequency of the double-resonance signal over time, an upper limit on the leak rate of the cells is obtained. The results are compared to the leak rate obtained with a membrane deflection method, applied to samples without rubidium. Further characterization of the cells and the bond showed the suitability of the alkali vapor cell for the use in chip-scale atomic clocks with the potential for combination with known anti-relaxation coatings.

II. FABRICATION OF ALKALI VAPOR CELLS

The studied cells are made from two silicon-glass preforms, bonded together by thermo-compression indium bonding. Indium is a soft metal (Moh's hardness of 1.2) with a melting temperature of 156 °C. It is well-known for its use in cryogenic and vacuum applications as hermetic sealing material. The natural oxide, which forms in ambient air, is very hard and renders bonding difficult.[17] However, if the oxide is broken and pure indium gets in contact with pure indium, a strong bond is formed.

In our cell design, the weak adhesion of In onto Si is improved by using a metallic adhesion intermediate layer. The metals are chosen to be the least disturbing for the clock operation, but at the same time, they should lead to a strong and hermetic bond. Chromium is chosen as the adhesion layer on silicon, and a thin gold layer protects it from oxidation. This protection is important since the indium is not applied in the same vacuum cycle as the chromium and does not wet chromium oxide, which forms instantly when chromium is exposed to air. The gold protection layer diffuses into indium as soon as indium is evaporated.[18] All the metals are applied by electron beam evaporation. The fabrication processes of both preforms and the sealing of alkali cells are depicted in Figure 1. The preforms are prepared at the wafer level, while the cells are filled with Rb and sealed at the chip level. Starting materials are two Pyrex wafers of 500 μm thickness and two double-sided polished silicon wafers of 390 μm thickness. The silicon wafers are etched down 500 nm, leaving arrays of two concentric 100 μm wide rings, which will later act as separation barriers between the

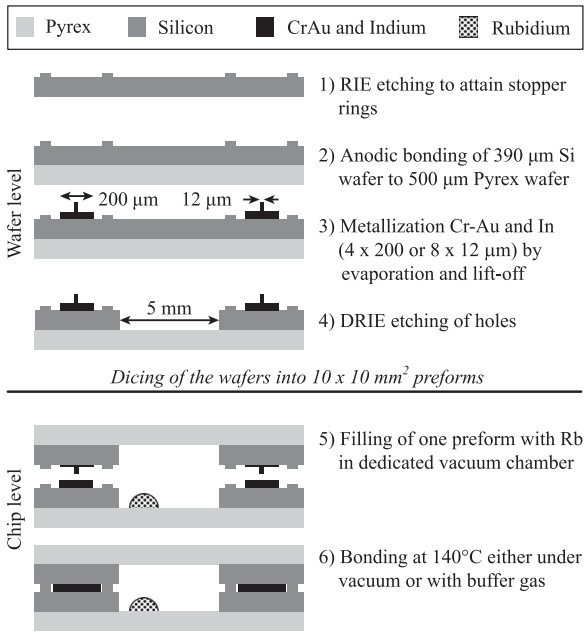

FIG. 1. Schematic of alkali cell fabrication and thermocompression sealing.

bond metal and the alkali metal and at the same time as stoppers for the compression during bonding. Two preform wafer stacks, each consisting of a Pyrex and a silicon wafer, are then formed by anodic bonding.

The Cr-Au adhesion rings with a diameter of 6 mm and 200 μm wide are first evaporated and patterned by lift-off process between the two 100 μm wide silicon rings. Through a second lift-off process, the indium bonding rings are created, 200 μm wide and 4 μm high on one wafer, merely 12 μm wide but 8 μm high on the other one. As a last step on wafer level, the holes are etched in the middle of the metallic rings by deep reactive ion etching (DRIE). The wafer stacks are then diced into $10 \times 10\,\mathrm{mm}^2$ preforms. The two preforms are cleaned in acetone for a few minutes, followed by a dip in isopropanol alcohol and are then blow dried with nitrogen. They are mounted on carriers in a vacuum chamber, which is pumped down to 10^{-7} mbar. Filling of a small amount of metallic Rb to the cells is accomplished by a previously reported method[14] using an alkali dispenser.

At this point, either a controlled amount (pressure) of a buffer gas mixture can be introduced or the cell can be sealed under high vacuum. For the sealing, the two preforms are brought into contact and heated up to 140 °C. As soon as the temperature is reached, 4×10^5 Pa tool pressure is applied. Due to the high aspect ratio of the top indium ring and the applied pressure, the strong natural oxide of the indium breaks up and the thin top ring also opens up the oxide layer on the bottom preform. This enables pure indium to get into contact with pure indium and hence to form a strong bond. The final cell is shown in Figure 2.

III. MECHANICAL VALIDATION OF THE BONDING PROCESS

Tensile tests carried out with samples bonded on chip level (i.e., containing metallic Rb) at 140 °C and with an

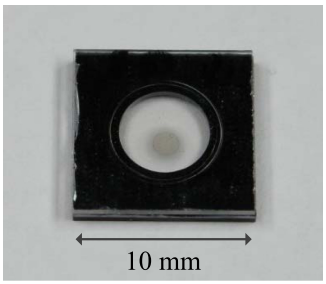

FIG. 2. Picture of an indium-bonded rubidium vapor cell. Metallic rubidium is clearly visible inside the 5 mm diameter inner cell volume.

applied tool pressure of 4×10^5 Pa show tensile strengths of 12 MPa, which is comparable to the values achievable with anodic bonding. The profiles of the metallization after tensile tests (see Figure 3) show that the actual bonding mostly happens where the narrow In ring of the top preform cuts into the bulk In of the bottom around 300 μm position in Figure 3(b) and 3(d).

Tests for gross leaks and the tensile strength of the bonding were carried out with simple test structures bonded on wafer level. Arrays of metallization rings as described above are created on single wafers. Those wafers were bonded in a wafer bonder (SussMicrotech SB6 E) using varying process parameters, then diced and tested. Compared to bonding on the chip level, wafer-level treatment with this bonder allowed for better alignment, improved parallelism, and higher tool pressure up to 8×10^5 Pa. For the gross leak test, the diced samples are kept in isopropanol alcohol for an hour. As isopropanol has a very low surface tension, it flows easily through small holes. Sample structures with the same metallization as described above reach the same tensile strength, with a yield of 96% of the test structures on one wafer, which passed the gross leak test in isopropanol alcohol. For samples where the number of the narrow In rings (12 μm wide in this case) on the top preform is increased from one to seven and the tool pressure doubled for bonding, tensile strength was measured to be increased by 50%. Figure 4(a) shows a scanning electron microscope (SEM) picture of the indium surface right before bonding, compared to Figure 4(b), which shows the surface after bonding and pull test. The observed differences give indications that through the pull tests the indium seals break in the bulk, and not at the initial surfaces nor at the interface indium-adhesion layer.

With samples bonded at wafer level at a temperature as low as 60 °C and an increased tool pressure of 8×10^5 Pa, tensile strength is also in the range of 12 MPa, which demonstrates the robustness of the technique and the potential for chip bonding at temperatures lower than 80 °C, the melting temperature of tetracontane, a highly effective anti-relaxation coating.

IV. SPECTROSCOPIC VALIDATION OF THE INDIUM-BONDED CELLS

Three spectroscopic methods were used to validate the indium-bonded Rb cells: linear absorption laser spectroscopy, saturated-absorption laser spectroscopy and laser-microwave double-resonance spectroscopy. An evacuated cell (containing only a droplet of rubidium but no buffer gas) and a buffer-gas filled Rb cell (150 mbar nominal pressure) were examined.

A. Linear spectroscopy

The presence of rubidium vapor inside the cells was confirmed for both the evacuated and the buffer-gas filled cell, by optical absorption spectroscopy on the Rb D_2 line at 780 nm (see Figure 5). In order to enhance atomic density and thus the contrast of the absorption, the cells were heated to 70 °C. The In-bonded evacuated cell shows narrow, only Doppler-broadened absorption lines indicating proper hermetic enclosure of atomic Rb. The buffer-gas cell shows collisional broadening and a negative frequency shift of the

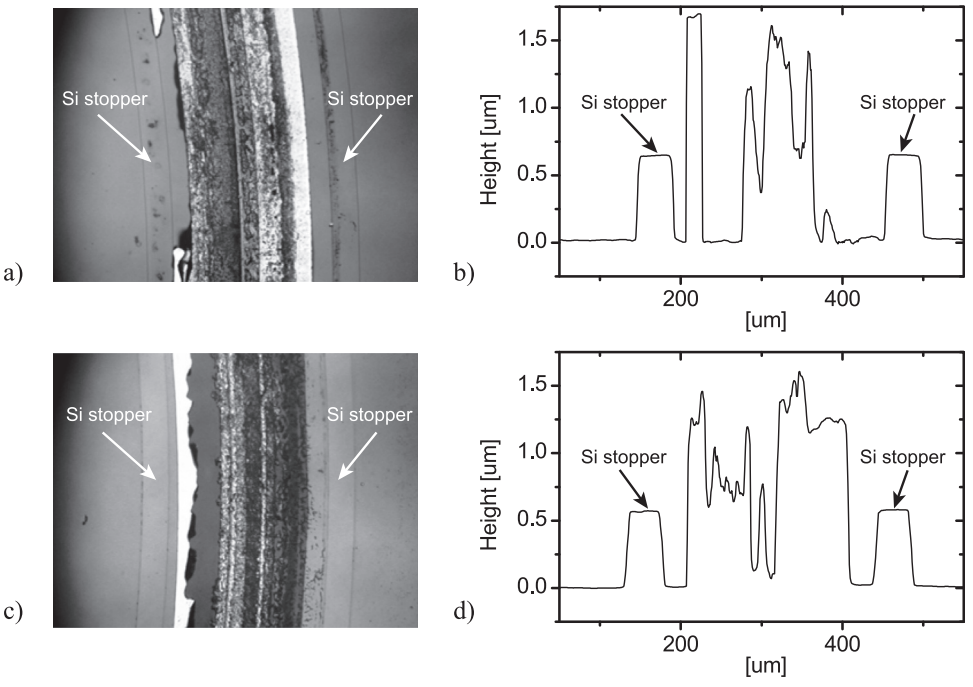

FIG. 3. (a) Intensity image of metallization of bottom preform after pull test (b) Profile of metallization of bottom preform after pull test. (c) Intensity image of metallization of top preform after pull test. (d) Profile of metallization of top preform after pull test.

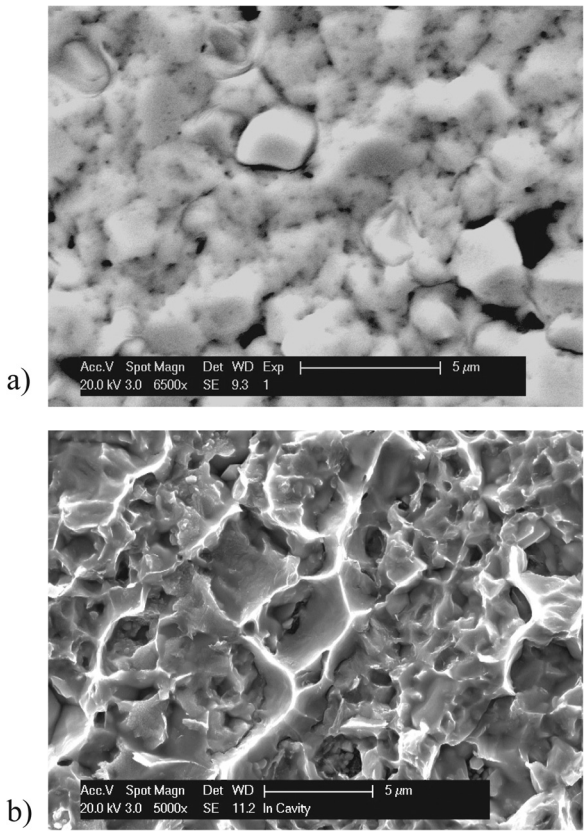

FIG. 4. SEM pictures of indium surface (a) before bonding and (b) after bonding and pull test.

absorption lines (both in the order of few MHz/mbar),[19] which confirms the presence of buffer-gas in this cell.

B. Saturated-absorption spectroscopy

Saturated-absorption spectroscopy[20] was performed on the evacuated cell in order to assess the cleanliness of the bonding process. Analyzing the width of the narrow Doppler-free lines (down to 6 MHz for a non-contaminated cell) allows to measure gas pressure inside the cell on the order of 1 mbar or below (assuming nitrogen gas contamination). Figure 6 shows the saturated-absorption spectrum for an indium-bonded cell (60 °C cell temperature) recorded 2

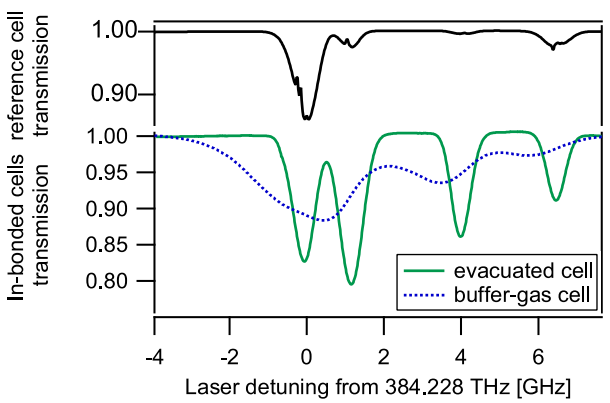

FIG. 5. Optical absorption spectra of two different In-bonded cells (bottom graph), compared to a reference cell (top graph). Broadening and shift of the absorption lines of the buffer-gas cell are due to the buffer-gas inside the cell.

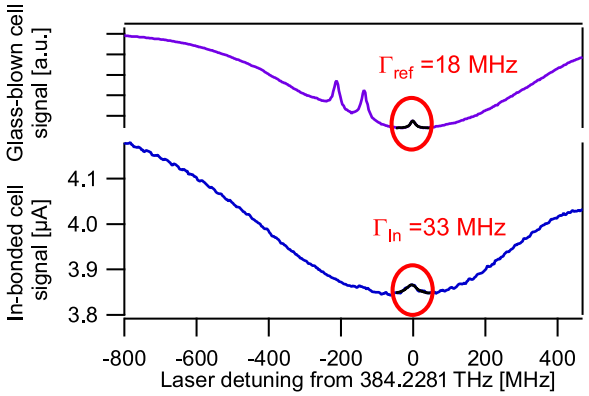

FIG. 6. Saturated-absorption spectrum of an indium-bonded cell (lower trace) compared to the one of a cm-scale glass-blown reference cell (upper trace). Circles mark the saturated-absorption line of the 87Rb $F = 2 \rightarrow F' = 3$ transition. Note that the strong saturated-absorption lines present for the cm-scale reference cell (cross-over resonances located at -133 and -211 MHz) are not observed in the In-bonded cell here.

months after sealing, and for a cm-scale glass-blown cell serving as reference, recorded under similar experimental conditions. Compared to the linewidth Γ_{ref} obtained from the glass-blown reference cell, which is limited by optical power broadening and the linewidth of the interrogating laser, the In-bonded cell showed an additional broadening of $\Gamma_{\mathrm{In}} - \Gamma_{\mathrm{ref}} = 15(4)$ MHz with respect to the cm-scale reference cell. This additional broadening can be interpreted as being due to gas contamination of the vapor cell. Since He and N_2, the most probable contaminants, have broadening coefficients of $\approx$15 MHz/mbar,[19] the gas contamination of the cell is estimated to be $\leq$1 mbar. Such gas pressures are high enough to significantly degrade the clock-transition linewidth in a cm-scale wall-coated vapor cell.[21] The same measurement was repeated 5 months after fabrication and no further broadening was detected, thus maintaining the same upper limit for a potential contamination. From the 4 MHz uncertainty of the linewidth result we derive an upper limit for a potential leak rate of 3×10^{-13} mbar·l/s.

C. Double-resonance spectroscopy

Laser-pumped double-resonance spectroscopy[2,22] was performed on a cell containing both Rb and a buffer-gas mixture (150 mbar pressure), to demonstrate the suitability of the cell for clock applications and to evaluate the leak rate of the In bonding. The cell was mounted on a double-resonance spectroscopy setup[22] to retrieve the resonance signal of the $5^2S_{1/2}\ |F = 1, m_F = 0\rangle \rightarrow |F = 2, m_F = 0\rangle$ clock transition. The setup (see Figure 7) consists of a compact, frequency-stabilized laser head that emits light resonant with the Rb D2 line at 780 nm, and a magnetron-type microwave cavity resonant at 6.834 GHz containing the cell under test. The microwave cavity is used to apply the microwave magnetic field to the atoms and is excited by a commercial synthesizer. The microwave cavity is also surrounded by a solenoid (C-field coil) in order to apply a static magnetic field, creating the quantization axis, and at the same time, isolating the "clock" transition by Zeeman splitting. The whole is surrounded by two layers of mu-metal magnetic shields to reduce the effect

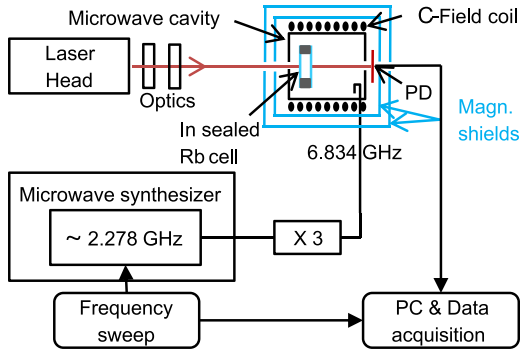

FIG. 7. Double-resonance atomic clock setup used for the experiments.

of external magnetic field fluctuations. The clock signal—as shown in the inset of Figure 8—is obtained by recording the light intensity transmitted through the cell while sweeping the microwave frequency. The signal linewidth extrapolated to zero light intensity is 2.022(7) kHz, only slightly higher than the predicted intrinsic linewidth of 1.6 kHz for our cell design,[10] most probably due to power broadening by the microwave field. The measured 16.8 kHz shift of the clock signal, as compared to the unperturbed resonance frequency, is in good agreement with the calculated shift of 16 kHz expected for the buffer-gas mixture ratio r theoretically filled into the cell ($r = P_{Ar}/P_{N_2} = 1.3$, $P_{tot} = 150$ mbar, in this case),[23] which shows good control of the filling procedure. A correction factor for the non-uniformity of the gas density within the filling chamber during cell sealing due to temperature differences between the cell and the pressure gauge was taken into account when calculating the shift.

V. LEAK RATE CHARACTERIZATION

In the presence of a leak with leak-rate L, the evolution of the pressure P inside a cell is proportional to the difference of internal and external pressures and can be expressed by

$$\frac{dP}{dt} = \frac{L}{P_{norm}V_0}(P_{ext} - P), \tag{1}$$

where V_0 is the volume of the cell cavity, P_{norm} a normalization pressure of 1000 mbar, and P_{ext} the external pressure at

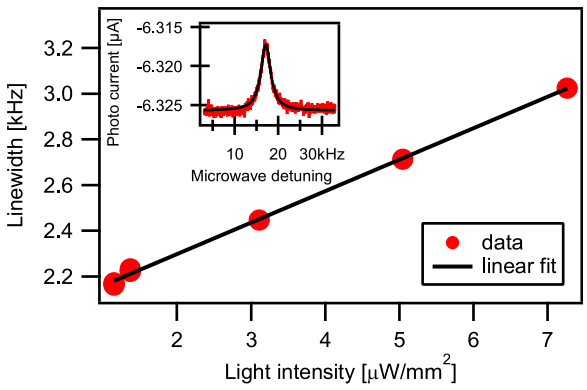

FIG. 8. Linewidth of the double-resonance clock signal of the In-bonded cell with buffer gas. The linewidth extrapolated to zero light intensity is 2022(7) Hz. The inset shows an example of the clock signal.

which the sample is kept (1000 mbar in our case). The pressure evolution is then

$$P(t) = P_{ext} - (P_{ext} - P_0)\cdot e^{-(Lt/VP_{norm})}, \tag{2}$$

where P_0 is the initial pressure inside the cell at $t = 0$. Since the expected pressure variations are small compared to the external pressure, a linear approximation can be made giving a much simpler expression for L

$$L = V\frac{\Delta p}{\Delta t}. \tag{3}$$

Frequency aging or drift of a miniature atomic clock should be on the level of 10^{-11}/day or less, which in the case of Rb and N_2 and our 15 μl cell volume corresponds to a leak rate of $\sim 5 \times 10^{-14}$ mbar·l/s (i.e., a total pressure change of 1 mbar over a 10 years lifetime). Such leak rates are difficult to measure over short periods of time; for example, the minimum leak rate measureable with standard helium leak test devices is on the order of 10^{-11} mbar·l/s. We therefore used two alternative methods to characterize the tightness of the In-bonding over time.

The first method was mechanical; it is based on the measure of the deflection of a Si membrane[24] integrated into dedicated cell samples. If the deflection is small compared to the size of the membrane, the membrane deflection can be linked to the pressure difference $P_D = P_{ext} - P$ between the two sides of the membrane. Using the analytical model of Bonnotte,[25] and assuming zero residual stress in the membrane, this difference is expressed as follows:

$$P_D = C_1\frac{bd^3}{a^4}\frac{E}{(1-\nu)} + C_2\frac{E}{(1-\nu^2)}\frac{b^3d}{a^4}, \tag{4}$$

where E is the Young's modulus and ν the Poisson ratio, b the thickness of the membrane, d the maximum deflection, and a half the side length of the square membrane. C_1 and C_2 are coefficients that depend on the shape and material of the membrane. In the case of a square membrane, we use $C_1 = 1.84$ and $C_2 = 4.129$, derived from the coefficients given by Timoshenko[26] for a thin square membrane with small deflections. Knowing the pressure outside the cavity P_{ext}, which corresponds to the atmospheric pressure, the internal pressure can be deduced from Equation (4). Assuming atmospheric pressure known within 0.1 mbar and the deflection within 10 nm, the detection limit for pressure changes would be about 1 mbar. The membrane deflections as well as the atmospheric pressure during the measurements were recorded right after bonding of the sample cells and thereafter every few weeks.

In order to observe a reasonably large membrane deflection, sample structures with thin membranes are prepared. They are fabricated by KOH etching of arrays of squares on a 525 μm silicon wafer. The wafers are removed from the etch bath when the membranes reach a thickness of about 40 μm with a side length close to 3 mm. The wafer with the cavities is bonded to a silicon wafer using the same metallization and the same bonding parameters as described above; the wafer

stack is then diced into 10×10 mm^2 chips. Since the bonding is done under vacuum, the membrane is deflected when exposed to ambient pressure as shown in Figure 9.

A white light interferometer (Wyko NT1100) was used to measure the deflection of the membranes, with measurements taking place over several months. No evident decrease in membrane deflection was observed over several months although the dependency of the deflection along with the atmospheric pressure P_{ext} could be seen easily. The pressure P inside the cavity was calculated by taking into account the variations of the atmospheric pressure over 5 months. The variation of the internal pressure was 1 mbar overall peak-to-peak value, with no trend observable. Taking into account the limited accuracy of both the interferometer (about 10 nm) and the atmospheric pressure sensor, we get a maximum change of 2 mbar over 5 months, which corresponds to a leak rate of 2.2×10^{-12} mbar·l/s. This is to be considered as an upper limit to a potential leak rate of the cells; measurements over longer time range are expected to further reduce this limit.

The second method was based on DR spectroscopy of a BG filled In-bonded cell. In addition to its quenching and anti-relaxation properties, the presence of a BG mixture also induces a shift from the unperturbed frequency on the microwave clock transitions that are proportional to each relative pressures of the gas considered[23]

$$\Delta\nu_{tot} = \sum_i \Delta\nu_i = \sum_i P_i(\beta_i + \delta_i \Delta T + \gamma_i \Delta T^2), \qquad (5)$$

where the indices i refer to the different BG considered, $\Delta\nu_i$ is the induced shift, P_i the partial gas pressure, and β_i, δ_i, and γ_i are coefficients proper to the gas and alkali atom considered. Thus, for identical experimental conditions, any income of buffer gas would lead to a shift proportional to the variation of the internal pressure. For a cell kept in air, one can assume that only nitrogen participates to an internal pressure increase, with a nitrogen pressure-shift coefficient of $\beta = 411$ Hz/mbar (Ref. 27), since oxygen—the second most probable contaminating gas—would immediately react with the alkali atoms. In order to correct for shifts caused by the light-atom interaction and extract the cell's intrinsic shift, a linear extrapolation of the clock frequency to zero light intensity was done for each measurement.

The clock frequency shift extrapolated to zero light intensity in the In-bonded cell was measured four times over the timespan of one year, and each point was then scaled to a pressure deviation from the first data point (see Figure 10), assuming a cell contamination by nitrogen only. The error bars include systematic shifts due to the positioning uncertainty of the cell inside the microwave resonator that may lead to varying microwave power shifts. However, an upper limit for a potential leak rate of the cells can still be estimated. Using the maximum pressure variation of ≈0.28 mbar over one year, we obtain a maximum leak rate of 1.5×10^{-13} mbar·l/s.

VI. DISCUSSION

All reported leak rate measurements for the In-bonded cells are in good agreement with each other, giving upper limits of 2×10^{-12} to 1.5×10^{-13} mbar·l/s. An increase in gas pressure within a sealed cell can have different origins: outgassing from the cell walls, flow of atmospheric gases into the cavity through potential micro-leaks in the bonding structure or cell walls, or permeation of gases (in particular He) through the cell walls.

If a pressure increase is measured right after bonding, it is most probably due to outgassing of trapped gases at the surfaces or in the bulk of the materials used, which are liberated at the bonding temperatures. Such outgassing can be limited by performing an outgassing step with the preforms before bonding. As the melting temperature of indium is very low, this step was not performed for the fabrication of the alkali cells presented in this paper, which could explain the small but non-zero gas pressure after bonding reported in Sec. IV B. In spite of the omitted outgassing, the saturated-absorption spectroscopy with the evacuated cells confirms a stable gas contamination of less than 1 mbar, which is acceptable for alkali buffer-gas cells. For an even cleaner

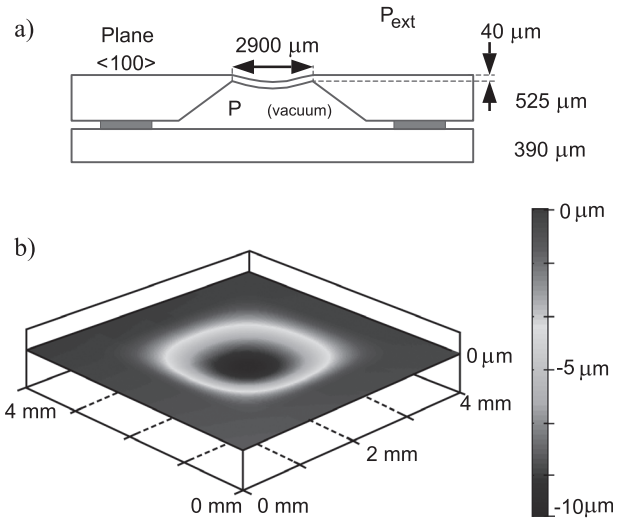

FIG. 9. (a) Schematic of test structures for optical leak rate testing by membrane deflection measurement. (b) Membrane profile of test vehicles after bonding in vacuum and exposed to atmospheric pressure measured with a white light interferometer.

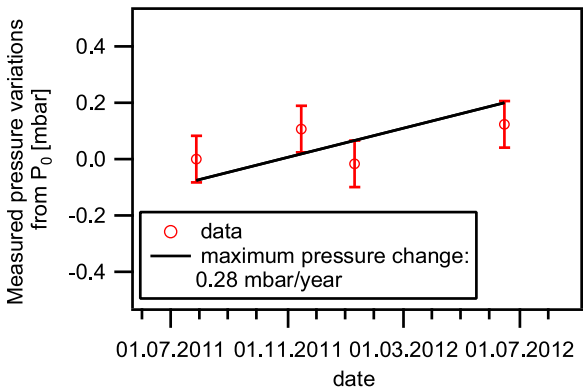

FIG. 10. Evolution of the clock transition frequency expressed as corresponding nitrogen pressure change, recorded at 70 °C over 5 months for a buffer-gas filled indium-bonded cell. Error bars include systematic uncertainties of the center frequency.

atmosphere, an outgassing step below the melting temperature of indium could be integrated in the process, or a getter material could be integrated.

If a steady increase of pressure is observed after bonding, it could still originate from outgassing but it might also arise from a leak of gases surrounding the cell into the sealed cavity. Even though indium is known as hermetic material, both the bonding interface and also the interface between the different metals can be the source for micro-leaks through which atmospheric gases might enter the cells. If such micro-leaks are small, small atmospheric gas molecules—such as He as the smallest gas molecules—may be expected to be the main source of gas contamination to the cell. In the case that such micro-leaks are large enough to let pass bigger atmospheric gas molecules, N_2 as the most abundant atmospheric gas is expected to be the main contaminant for the cell. The clock transition's pressure shift coefficients for N_2 (411 Hz/mbar [Ref. 23]) and for He (540 Hz/mbar [Ref. 27]) differ by about 25% only, but due to the high abundance of N_2 in the atmosphere, the impact of a potential N_2 contamination of the cell on the clock frequency is expected to be dominant, which motivates the analysis in Sec. V. Furthermore, such leakage process should be accompanied by a cell contamination with O_2 and H_2O and subsequent oxidation of the alkali metal. However, oxidation of the rubidium was not yet observed during the measurements reported in Figure 10.

It has been shown previously that He gas can permeate through the walls of glass-blown alkali vapor cells, which can impact the aging behavior of vapor cell atomic clocks,[27] while permeation rates of other atmospheric gases are smaller by factors of 50 (Ne) to more than 7 orders of magnitude (Ar, O_2, N_2).[28] This permeation process includes the steps of gas adsorption on the wall surface, its solution in and diffusion through the cell walls, and finally desorption from the inner cell walls.[28] Table I summarizes the key parameters for He permeation through Pyrex glass and Si (the two main materials used in our cells), i.e., the solubility S, diffusion constant D, and Permeation rate $K = S{\cdot}D$,[29] for a temperature of $T = 100\,^{\circ}C$. As permeation of He through Si is smaller by many orders of magnitude compared to permeation through Pyrex, it is negligible here. It is therefore sufficient to treat the permeation through the Pyrex windows only.

For the 15 μl volume cell design studied here, the total Pyrex window surface is 0.4 cm^2 and it can be estimated[30] that the total He permeation leak rate through the windows is $L_{He} \approx 2 \times 10^{-9}$ mbar·l s^{-1}. For the model case of a more drastically miniaturized 1 μl volume cell with 1 mm^2 window surface, the total He permeation leak rate is expected to be $L_{He} \approx 1 \times 10^{-10}$ mbar·l s^{-1}. Using Eqs. (2) and (3), the initial pressure change rate $\Delta P/\Delta t$ (using the partial atmospheric He pressure $P_{ext} = 5.3 \times 10^{-3}$ mbar) and the He permeation time constant $\tau_{He} = V\ P_{norm}/L_{He}$ for the He pressure increase in the cell can be calculated and are given in Table II for the two cells designs. For our present cell design, we find $\tau_{He} = 72$ days which is of the same order as reported in Ref. 27 for cm-scale all-glass cells with 0.5 mm wall thickness. After one year, the total pressure inside our cells due to He permeation is calculated to be only 1% lower than the atmospheric He partial pressure, which is far below the pressure change reported in Figure 10. For the case of the 1 μl cell, the permeation time constant is $\tau_{He} = 96$ days.

TABLE I. Solubility, diffusion constant and permeation rate of He through Pyrex and crystalline Si, for a temperature of 100 °C. The Si data were obtained by extrapolating the data of Van Wieringen *et al.*[31]

	Solubility S (cm^3/cm^3 at 1 atm)	Diffusion constant D ($cm^2\ s^{-1}$)	Permeation rate K ($m^2\ s^{-1}\ Pa^{-1}$)
He through Pyrex[a]	4.3×10^{-3}	7.0×10^{-8}	3.0×10^{-19}
He through Si[b]	8.5×10^{-12}	1.1×10^{-18}	9.2×10^{-39}

[a]Reference 29.
[b]Reference 31.

TABLE II. Calculated initial pressure change rate $\Delta P/\Delta t$ and permeation time constant for the 15 μl cell studied here and a hypothetical 1 μl cell. Pyrex window thickness is 0.5 mm in both cases. Parameters of Table I were used.

Cell design	Initial pressure change rate $\Delta P/\Delta t$	He permeation time constant τ_{He}
15 μl cell (see Sec. II)	7.3×10^{-5} mbar/day	72 days
1 μl cell	5.5×10^{-5} mbar/day	96 days

We thus conclude that a potential pressure increase of 0.28 mbar over one year—the most stringent upper limit from our measurements—cannot be explained by He permeation through the cell windows, nor by He entering the cell volume via small leaks as the measured upper limit is far above the atmospheric He partial pressure. A pressure increase on this level—if confirmed to be real—needs to be interpreted as being due to leakage of more abundant atmospheric gases (mainly N_2) into the cells or continued outgassing. The small pressure potentially present after cell sealing (cf. Sec. IV B) can be explained by outgassing during sealing of the cells.

A decrease in optical or double-resonance signal amplitude would indicate a decrease in the alkali vapor pressure and could be a sign of rubidium interacting with the metallic layers or diffusion through it, rather than leakage of water or oxygen into the cavity. Even though such a decrease in signal was not yet observed, it cannot be excluded that such chemical interaction might happen if the cell is kept at the clock working temperature for longer time. In order to separate this effect from a possible gas leakage through the indium seal at elevated temperature, it would be of interest to conduct leak rate measurements on cells with and without rubidium at higher temperatures.

For the reported studies, the alkali vapor cells were maintained at room temperature for most of the time and were only heated up to ~70 °C for the spectroscopic measurements. This accumulated to a total of less than 500 h at elevated temperature. When operating the cells over longer time at elevated temperature, there might be the possibility of rubidium diffusing into the indium or reacting slowly with the metallic seals. This process was not addressed in the present work and remains to be studied.

VII. CONCLUSION

We have demonstrated the fabrication and evaluation of micro-fabricated alkali vapor cells, sealed by thin-film indium thermo-compression bonding. This technique yields tensile strengths of the resulting bond comparable to the commonly used anodic bonding technique. Results from optical spectroscopy confirm a stable and sufficiently clean atmosphere inside the cell, in spite of the somewhat limited compatibility of the indium bonding technique with outgassing of the preforms before bonding (due to the low melting temperature of indium). A consistent upper limit of 1 mbar was found for a potential gas contamination inside the cells during the sealing and over the time of several months, proving a clean process and also the good hermeticity of the indium bonding.

The suitability of the cells for atomic clock applications was demonstrated by recording double-resonance signals for a buffer-gas filled In-bonded cell. The retrieved clock signal linewidth is 2.02 kHz, only slightly higher than the theoretically predicted intrinsic linewidth for this cell. The center frequency of the cell was recorded several times over the course of one year, giving an upper limit of 1.5×10^{-13} mbar·l/s^{-1} for a potential leak rate. This result is compatible with the results obtained from the membrane deflection method performed on samples without alkali metal present. An analysis of He permeation through the cell walls shows that this process corresponds to a pressure variation in the cell around 3 orders of magnitude smaller than our experimental upper limit.

The low-temperature hermetic sealing technique demonstrated here presents a clear improvement compared to previously reported low-temperature sealing techniques. With sealing temperatures below 140 °C, thin-film indium sealing is already compatible with anti-relaxation coatings such as OTS, and opens the way towards microfabricated wall-coated alkali vapor cells for applications such as atomic clocks or magnetometers. By exploiting the demonstrated higher bonding pressures up to 8×10^5 Pa, cell sealing at temperatures below the melting temperature of micro-fabricated alkali cells with paraffin-type wall-coatings is also expected to be possible.

ACKNOWLEDGMENTS

This work was supported by the Swiss National Science Foundation (Sinergia Grant No. CRSI20-122693/1). The authors thank the CMI and the CSEM Microsystems Technology Division staff and all the Sinergia project partners for their contributions and help. They also acknowledge the contributions from C. Schori and P. Thomann at the early stages of the project.

[1] S. Knappe, Comprehensive Microsyst. **3**, 571 (2008).
[2] J. Camparo, Phys.Today **60**(11), 33 (2007).
[3] L.-A. Liew, S. Knappe, J. Moreland, H. Robinson, L. Hollberg, and J. Kitching, Appl. Phys. Lett. **84**, 2694 (2004).
[4] K. Tsujimoto, Y. Hirai, K. Sugano, T. Tsuchiya, and O. Tabata, in *Proceedings of the 25th IEEE International Conference on Micro Electro Mechanical Systems, MEMS 2011*, Cancun, Mexico, 23–27 January 2011, pp. 368–371.
[5] Y. W. Yi, H. G. Robinson, S. Knappe, J. E. Maclennan, C. D. Jones, C. Zhu, N. A. Clark, and J. Kitching, J. Appl. Phys. **104**, 023534 (2008).
[6] G. Robinson and C. E. Johnson, Appl. Phys. Lett. **40**, 771 (1982).
[7] D. Budker, L. Hollberg, D. F. Kimball, J. Kitching, S. Pustelny, and V. V. Yashchuk, Phys. Rev. A **71**, 012903 (2005).
[8] S. J. Seltzer, D. M. Rampulla, S. Rivillon-Amy, Y. J. Chabal, S. L. Bernasek, and M. V. Romalis, J. Appl. Phys. **104**, 103116 (2008).
[9] T. Bandi, C. Affolderbach, and G. Mileti, J. Appl. Phys. **111**, 124906 (2012).
[10] J. Kitching, S. Knappe, and L. Hollberg, Appl. Phys. Lett. **81**, 553 (2002).
[11] A. Douahi, M. Hasegawa, L. Nieradko, J. J. Boy, C. Gorecki, and V. Giordano, in *Proceedings of the 22nd European Frequency and Time Forum (EFTF)*, Toulouse, France, 22–25 April 2008, FPE-0061.
[12] C. Rahman and H. Robinson, IEEE J. Quantum Electron. **23**, 452 (1987).
[13] S. J. Seltzer and M. V. Romalis, J. Appl. Phys. **106**, 114905 (2009).
[14] Y. Pétremand, C. Schori, R. Strässle, G. Mileti, N. de Rooij, and P. Thomann, in Proceedings of at the 2010 European Frequency and Time Forum (EFTF), Noordwijk, Netherlands, 13–16 April 2010, P119.
[15] R. Straessle, M. Pellaton, Y. Pétremand, C. Affolderbach, D. Briand, G. Mileti, and N. F. de Rooij, in *Proceedings of the 26th IEEE International Conference on Micro Electro Mechanical Systems, MEMS 2012*, Paris, 29 January – 2 February 2012, pp. 361–364.
[16] R. Straessle, Y. Petremand, D. Briand, N. F. de Rooij, M. Pellaton, C. Affolderbach, and G. Mileti, in *Proceedings of the IEEE International Frequency Control Symposium (FCS)*, Baltimore, MD, USA, 21–24 May 2012, pp. 127–130.
[17] J. Kim, H. Schoeller, J. Cho, and S. Park, J. Electron. Mater. **37**, 483 (2008).
[18] V. Simić and Ž. Marinković, Thin Solid Films **41**, 57 (1977).
[19] M. D. Rotondaro and G. P. Perram, J. Quant. Spectrosc. Radiat. Transfer **57**, 497 (1997).
[20] S. A. Knappe, H. G. Robinson, and L. Hollberg, Opt. Express **15**, 6293 (2007).
[21] S. Knappe and H. G. Robinson, New J. Phys. **12**, 065021 (2010).
[22] M. Pellaton, C. Affolderbach, G. Mileti, Y. Pétremand, and N. F. de Rooij, in *Proceedings of the 2011 Joint Meeting of the European Frequency and Time Forum (EFTF) and the IEEE International Frequency Control Symposium (IFCS)*, San Francisco, CA, 2–5 May 2011, pp. 604–606.
[23] J. Vanier, R. Kunski, N. Cyr, J. Y. Savard, and M. Têtu, J. Appl. Phys. **53**, 5387 (1982).
[24] D. Lellouchi, J. Dhennin, X. Lafontan, D. Veyrie, J.-F. L. Neal, and F. Pressecq, J. Micromech. Microeng. **20**, 025031 (2010).
[25] E. Bonnotte, P. Delobelle, L. Bornier, B. Trolard, and G. Tribillon, J. Mat. Res **12**, 2234–2248 (1997).
[26] S. P. Timoshenko and S. Woinowsky-Krieger, *Theory of Plates and Shells*, 2nd ed. (McGraw-Hill, New York, NY, 1959).
[27] J. C. Camparo, C. M. Klimcak, and S. J. Herbulock, IEEE Trans. Instrum. Meas. **54**, 1873 (2005).
[28] F. J. Norton, J. Appl. Phys. **28**, 34 (1957).
[29] K. Kawasaki and K. Senzaki, Jap. J. Appl. Phys. **1**, 223 (1962).
[30] G. L. Harding, Sol. Energy Mater. **5**, 141 (1981).
[31] A. Van Wieringen and N. Warmoltz, Physica **22**, 849 (1956).